processes

MDPI

Article

Cavity Size Effect on Host-Guest Property of Tiara-like Structural $M_n(SR)_{2n}$ Nanoclusters Probed by NMR Spectroscopy

Changlin Zhou, Shida Gong, Jishi Chen * and Zonghua Wang *

Shandong Sino-Japanese Center for Collaborative Research of Carbon Nanomaterials, College of Chemistry and Chemical Engineering, Instrumental Analysis Center of Qingdao University, Qingdao University, Qingdao 266071, China

* Correspondence: chenjishi@qdu.edu.cn (J.C.); wangzonghua@qdu.edu.cn (Z.W.)

Abstract: The lack of detect technology hinders the understanding of host-guest (H-G) chemical properties for thiolate-protected tiara-like structural nanoclusters ($M_n(SR)_{2n}$). In this work, NMR spectroscopy is demonstrated as a powerful tool to probe the H-G structure of $M_n(SR)_{2n}$ both experimentally and theoretically. A low-field shifting and wide chemical shift (CS) signal of the H nucleus in CH_2Cl_2 is observed in the NMR spectrum of the mixture of CH_2Cl_2 and $Pd_8(PET)_{16}$ (PET is 2-phenylethanethiol), agreeing with the theoretical results that a deshielding area appears in the central cavity of $Pd_8(SR)_{16}$. All $M_n(SR)_{2n}$ own similar nucleus-independent chemical shift maps and deshielding cavities, which means that the H nucleus in small molecules trapped by $M_n(SR)_{2n}$ should have consistent low-field shifted CSs. However, such a phenomenon was only observed in the NMR spectrum of the mixed solution of $Pd_8(SR)_{16}$ and CH_2Cl_2, indicating that $Pd_8(SR)_{16}$ is the only one in the series of $Pd_n(SR)_{2n}$ (n = 4~16) analogues that can capture a CH_2Cl_2, the H-G properties of $M_n(SR)_{2n}$ are highly dependent on their cavity sizes, and a guest molecule only inserts into the matching cavity of $M_n(SR)_{2n}$. We anticipate that the realization of such convenient probe strategy will give a deeper understanding of the H-G properties of $M_n(SR)_{2n}$.

Keywords: tiara-like structure; cavity size effect; $M_n(SR)_{2n}$; host-guest property; NMR

Citation: Zhou, C.; Gong, S.; Chen, J.; Wang, Z. Cavity Size Effect on Host-Guest Property of Tiara-like Structural $M_n(SR)_{2n}$ Nanoclusters Probed by NMR Spectroscopy. *Processes* **2022**, *10*, 2683. https://doi.org/10.3390/pr10122683

Academic Editor: Alexander S. Novikov

Received: 24 November 2022
Accepted: 10 December 2022
Published: 13 December 2022

1. Introduction

A unique tiara-like framework endows thiolate-protected group 10 transition-metal nanoclusters ($M_n(SR)_{2n}$ (M is Ni, Pd, or Pt), an inorganic analogy of metallocrowns, with excellent physical and chemical properties, such as nonlinear absorption, stability, photoluminescence, catalytic performance, and host-guest (H-G) chemical properties [1–8]. $M_n(SR)_{2n}$ were considered potential host molecules since $Ni_6(SC_2H_5)_{12}$ was structurally determined [9]. The H-G structure of $M_n(SR)_{2n}$ was first experimentally determined in 2002 by the reporting of a tetrahydrofuran that was captured by $Ni_{11}(SC_6H_5)_{22}$ [10]. Then, several G@$M_n(SR)_{2n}$ (G denotes the guest molecule) were reported, including benzene and toluene molecules inserted into $Ni_{10}(SR)_{20}$ [3,11], a guest Ag^+ ion accommodated in $Pt_6(SR)_{12}$ [12], and $Pd_8(SR)_{16}$ or $Pt_8(SR)_{16}$ encapsulating a small molecule, such as CH_2Cl_2, CH_2Br_2, CH_2ClCH_2Cl, CH_3I, and I_2 [13,14]. To the best of our knowledge, single crystal X-ray diffraction (SCXRD) is the only technique to obtain the H-G structures of G@$M_n(SR)_{2n}$.

As we know, the size of the cavity in a host molecule plays a very prominent role in the formation of the H-G structure. Until now, $M_n(SR)_{2n}$ with various metal atoms, including $Ni_n(SR)_{2n}$ (n = 4~6, 8~12) [3,10,15,16], $Pd_n(SR)_{2n}$ (n = 4~20) [17], and $Pt_n(SR)_{2n}$ (n = 5~13) [1], were synthesized and isolated, but their large, high-quality single crystals, especially for the larger sized ones, were difficult to grow [18]. This is a huge obstacle to correlate their cavity sizes to H-G chemical properties using SCXRD. Therefore, it is highly desirable to develop an alternative analytical method for probing the H-G structure of

$M_n(SR)_{2n}$ without a single crystal sample. The NMR technique was used to detect the H-G properties for a large number of materials [19–24]. For example, Hu et al. confirmed that the stereoselective, guest-driven, self-assembly of either Λ4- or Δ4- type Eu4L4 cages has been realized via chiral induction with R/S-BINOL or R/S-SPOL templates by NMR [20]. Schäfer et al. revealed the existence of a complex dynamic equilibria of oligomers that are formed by the host with bidentate guests based on diffusion NMR spectroscopy [21]. Mi et al. used solid-state NMR to ensure that the ratio of two host and guest molecules is 1:1:2 in interheteromacrocyclic hosts charge transfer crystals [23]. However, none has been reported for $M_n(SR)_{2n}$ thus far, which may be due to the complexity of their guest molecules, including the metal ion (Ag^+), the small organic molecules, and the reductive inorganic molecule (I_2). In this work with $Pd_8(SR)_{16}$ and CH_2Cl_2 as model host and guest molecules (Scheme 1), NMR spectroscopy is shown to be a highly effective approach to confirm the H-G structure of $M_n(SR)_{2n}$ both experimentally and theoretically. Furthermore, we use NMR spectroscopy to study the size-dependent characteristics of host $Pd_n(SR)_{2n}$ NCs capturing guest molecules. In the future, we plan to use NMR spectroscopy for the detection of $M_n(SR)_{2n}$ capturing other molecules and expand their applications based on their H-G properties.

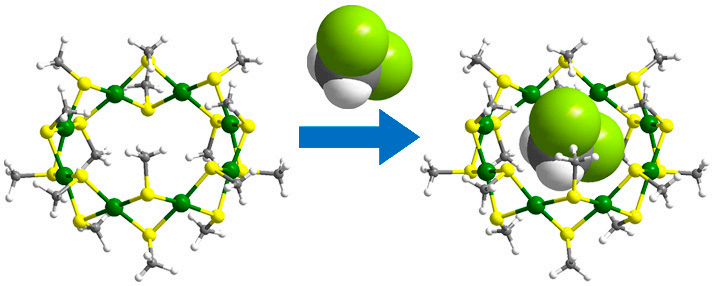

Scheme 1. A CH_2Cl_2 molecule inserts into the central cavity of $Pd_8(SCH_3)_{16}$. Color labels: green, Pd; yellow, S; light green, Cl; grey, C; white, H.

2. Materials and Methods

2.1. Materials

All reagents were commercially available and used as received. Palladium nitrate, sodium trifluoroacetate, and triethylamine were purchased from Sinopharm Chemical Reagent Co., Ltd, Shanghai, China. 2-phenylethanethiol, deuterochloroform, and trans-2-[3-(4-tert-butylphenyl)-2-methyl-2-propenylidene] malononitrile (DCTB) were purchased from Adamas, Shanghai, China.

2.2. Synthesis and Purification of $Pd_n(PET)_{2n}$

The synthesis of thiolate-protected palladium nanoclusters followed that of a previous report [17]. We dissolved 0.2 g $Pd(NO_3)_2{\cdot}2H_2O$ in 12 mL acetonitrile. After stirring for 30 min, 210 μL 2-phenylethanethiol was added into the above solution. Then, the reaction mixture was stirred for another 15 min, and 0.5 mL triethylamine was rapidly added. The reaction was allowed to continue under constant stirring for 5 h. After the reaction stopped, the yellow precipitate was washed several times with methanol and water, and then collected by centrifugation. The crude product was dissolved in CH_2Cl_2, and the precipitate consisting of insoluble Pd-thiolates was removed. The as-obtained soluble product was further isolated via thin-layer chromatography. Each $Pd_n(PET)_{2n}$ NC was purified by TLC for a minimum of three times.

2.3. Characterization

Matrix-assisted laser desorption ionization time-of-flight mass spectrometry (MALDI-TOF-MS) was collected by an autoflex speed TOF/TOF mass spectrometer (Bruker, Billerica, MA, USA) in reverse positive mode with DCTB used as the matrix. The ^{1}H NMR and 2D COSY of the mixture of $Pd_n(PET)_{2n}$ ($5 \leq n \leq 16$) and CH_2Cl_2 were recorded on a Bruker

400 MHz spectrometer (Billerica, MA, USA) at room temperature. Approximately 10 mg of each nanocluster was dissolved in 1 mL $CDCl_3$ containing 0.1 µL of CH_2Cl_2 (approximately 1.6×10^{-3} mmol) (tetramethylsilane was used as internal standards).

2.4. Calculational Details

The geometrical structure of $Pd_8(SCH_3)_{16}$, simplified by replacing the $-CH_2CO_2CH_3$ groups of the experimentally obtained $Pd_8(SCH_2CO_2CH_3)_{16}$ molecule with methyl groups, was used for the theoretical calculation. All theoretical calculations were carried out by the Density Functional Theory (DFT) method using the Gaussian 16 program (Revision B01) [25]. The selected functional was the hybrid-GGA functional B97-2 [26], which reaches rather constantly the lowest standard deviations among several common functionals [27]. The employed basis sets were the pcSseg-1 (for C, H, and S atoms), which are developed and optimized for NMR calculations [28], and the Stuttgart–Dresden double-ζ (SDD) with an effective core potential (ECP) (for Pd atoms) [29].

The nucleus-independent chemical shift (NICS) maps of the studied $Pd_8(SCH_3)_{16}$ toroid structure were carried out by calculating the isotropic shielding value ($\delta_{(r)}$) and its ZZ component ($\delta^{zz}{}_{(r)}$) of 132,528 points in the space of 6.348 Å (12 Bohr) extension of the molecular coordinate [30]. These $\delta_{(r)}$ and $\delta^{zz}{}_{(r)}$ values were used to generate the maps to denote the shielded (negative) and deshielded (positive) areas of the system by using the Multiwfn program (Revision 3.6) [31].

In the calculation, an external magnetic field ($\boldsymbol{B}^{\mathbf{ext}}$) of 1.0 T was applied perpendicular to the molecular plane, the induced magnetic field ($\boldsymbol{B}^{\boldsymbol{ind}}$, in ppm units) over the space was related with the shielding tensor $\boldsymbol{\sigma}$ and the external magnetic field $\boldsymbol{B}^{\mathbf{ext}}$, as was given elsewhere:

$$\boldsymbol{B}^{\boldsymbol{ind}}_{(r)} = -\boldsymbol{\sigma}_{(r)}\boldsymbol{B}^{\mathbf{ext}}$$

The isotropic shielding value $\delta_{(r)}$ (in units of ppm) can be determined by the definition:

$$\delta_{(r)} = \mathrm{NICS} = -\frac{1}{3}\mathrm{Tr}\boldsymbol{\sigma}_{(r)}$$

where $\mathrm{Tr}\boldsymbol{\sigma}_{(r)}$ represents the trace of the nuclear shielding tensor.

3. Results and Discussion

The host $Pd_8(SR)_{16}$ molecule was synthesized utilizing a procedure from a previous report [17]. In previous reports, a toluene molecule inserted into the $Ni_{10}S_{20}$ framework of $Ni_{10}(S\mathit{t}Bu)_{10}(SR)_{10}$ with 2-ethylthioethanethiol, 2-(2-mercaptoethyl)pyridine or 2-aminoethanethiol as perpendicular thiols [3,11], indicated that the H-G properties of $M_n(SR)_{2n}$ were not dependent to their thiolate ligands. To avoid the formation of an intramolecular H-G structure by the thiolate carbon chain entering the $Pd_8(SR)_{16}$'s central cavity [16], 2-phenylethanethiol (PET), a thiol owning a large carbon tail (the outer diameter of phenyl (~5.3 Å) is larger than the cavity size of the Pd_8S_{16} framework (~5.1 Å) [13]), was used as the ligand when we conducted the synthesis. The $Pd_8(PET)_{16}$ was synthesized and purified via a previous route [17]. Its chemical composition was identified by MALDI-TOF-MS and NMR, as shown in Figures 1 and S1. The only peak centered at 3062.8 Da in the MS spectrum, and the perfect agreement between the experimental and simulated isotopic patterns indicated that the $Pd_8(PET)_{16}$ sample was of high purity (Figure S1). In the ^{1}H NMR and COSY spectra (Figure 1), the three intriguing triplets at 2.6–3.2 ppm were assigned to the protons of the methylene groups (1 and 2 in Figure 1) within 2-phenylethanethiolate, and the peaks at 6.8–7.3 ppm corresponded to the phenyl groups (3–5 in Figure 1). The wide blank span at 3.4–6.8 ppm in the ^{1}H NMR spectrum would be an ideal window to observe the CS shift of the H nuclei within a guest molecule.

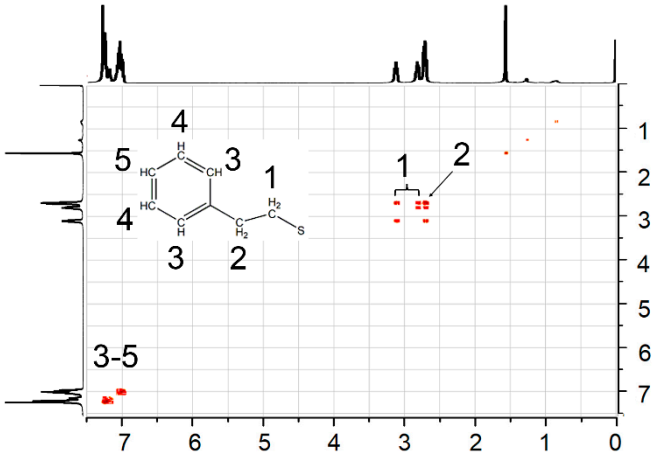

Figure 1. 2D COSY spectra of $Pd_8(PET)_{16}$ nanoclusters (room temperature, $CDCl_3$ as solvent).

Comparing four previously reported organic guest molecules of $Pd_8(SR)_{16}$, CH_2Cl_2, a cheap and easily available solvent, was optimized for the experiment. The reasons are as follows: First, its CS at 5.3 ppm [25] was in the middle of the observation window of $Pd_8(PET)_{16}$ and not disturbed by 2-phenylethanethiolate protected metal nanoclusters, e.g., $Ni_6(PET)_{12}$ [32], a small size $M_n(SR)_{2n}$; and second, unlike other guest molecules disordered in the central cavity of $Pd_8(SR)_{16}$ [13], there was only one configuration in which one C-Cl bond was arranged vertically and another one was nearly horizontal when CH_2Cl_2 was encapsulated by $Pd_8(SR)_{16}$ [13], as shown in Scheme 1. It should be noted that $CDCl_3$ was used as the solvent to characterize ^1H NMR because it cannot insert into $Pd_8(SR)_{16}$ [13]; this would be an effective strategy to avoid the competition between solvent and guest molecules in tests.

To obtain the CS changes of the CH_2Cl_2 molecules before and after entering $Pd_8(PET)_{16}$, the ^1H NMR spectra of pure CH_2Cl_2, pure $Pd_8(PET)_{16}$, and their mixture in $CDCl_3$ solution were compared first. In the mixture solution, the molar ratio of $Pd_8(PET)_{16}$ to CH_2Cl_2 was 2:1, ensuring that all CH_2Cl_2 molecules could insert into $Pd_8(PET)_{16}$. The ^1H NMR spectra of pure CH_2Cl_2, pure $Pd_8(PET)_{16}$, and their mixture in $CDCl_3$ solution are compared in Figures 2 and S2. The pure $Pd_8(PET)_{16}$ and the mixture solutions have the same CS signals of the H nuclei within $Pd_8(PET)_{16}$, but there were two changes in the H nuclei's CS within CH_2Cl_2 between the pure CH_2Cl_2 and the mixture solutions. One change was the CS of CH_2Cl_2 in the mixture moving toward low field (0.07 ppm). As shown in Figure 2a, unlike the CS of pure CH_2Cl_2 at 5.30 ppm [33], there was only one single, central peak at 5.37 ppm corresponding to CH_2Cl_2 in the ^1H NMR spectrum of the mixture. Another change was the CS signal of CH_2Cl_2 in the mixture solution owning a wider full width at half maximum (FWHM). As shown in Figure 2b,c, the FWHM of the mixture is approximately 0.0220 ppm, which is ~8.5 fold wider than that of pure CH_2Cl_2 (approximately 0.0026 ppm).

To verify the theory that the CS of H within CH_2Cl_2 shifting to low field was caused by CH_2Cl_2 inserted into $Pd_8(PET)_{16}$, we drew the NICS map of the host $Pd_8(SR)_{16}$ molecule to understand its magnetic response under an extra magnetic field. The structure of $Pd_8(SCH_3)_{16}$ (Scheme 1), simplified from the crystal structure of $Pd_8(SCH_2CO_2CH_3)_{16}$ [13], was used to carry out the calculation. After analyzing the crystal structures of $M_n(SR)_{2n}$ [19–21,34], especially $Pd_8(SR)_{16}$ [13,14,35], with or without guest molecules (Table 1), two main factors were taken into account when we used the simplified structure: First, the structural features of $M_n(SR)_{2n}$, such as the tiara-like framework, bond length and angles, and spatial arrangements of α-CH_2 (the methylene attached to the S atom), were slightly affected by their ligand species and guest molecule species; and second, for most H-G structures of $G@M_n(SR)_{2n}$, the ability of the host $M_n(SR)_{2n}$ trapping guest molecules into their specific M_nS_{2n} toroids was independent of their thiolate ligands. So it was reasonable that we considered the nearest segments of $M_n(SR)_{2n}$ to the guest molecule, including the M_nS_{2n}

framework and the α-CH_2, when we conducted the calculation. Theoretical induced magnetic fields of 132,528 points around the $Pd_8(SCH_3)_{16}$ were performed to investigate the isotropic magnetic response of this area. The NICS maps for $Pd_8(SCH_3)_{16}$ are shown in Figure 3. As shown in Figure 3a, the $\delta_{(r)}$ values in the areas nearby and outside of the molecular framework of $Pd_8(SCH_3)_{16}$ were negative and slightly positive, indicating that these areas are shielded and slightly deshielded regions, respectively. The $\delta_{(r)}$ values in the central cavity of the Pd_8 ring were positive (dark blue), showing that the cavity is a deshielded area. From Figure 3b, the deshielded area could be further understood as a closed area (inside the bold solid black line) surrounded by the $Pd_8(SCH_3)_{16}$ molecule. This closed, deshielded area could be characterized better by the positive values of the ZZ component of $\delta_{(r)}$ ($\delta^{zz}{}_{(r)}$ values, see Figure 3c,d). Therefore, one can infer that, once a small molecule is captured by $Pd_8(SCH_3)_{16}$, the resonant frequency of the H nuclei within the guest molecule will move towards the low field under an external magnetic field, showing that the CS of CH_2Cl_2 in the mixture moving towards low field was caused by the CH_2Cl_2 inserting into the central cavity of $Pd_8(PET)_{16}$.

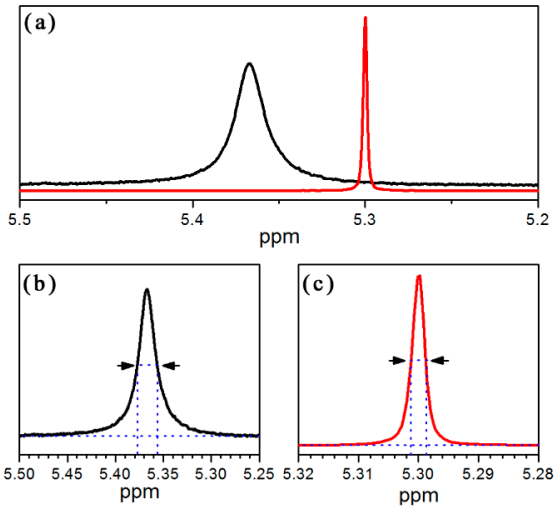

Figure 2. (**a**) ^{1}H NMR spectra, (**b**,**c**) the FWHMs of CH_2Cl_2; the black line is the mixture of $Pd_8(PET)_{16}$ and CH_2Cl_2, and the red line is the pure CH_2Cl_2 ($CDCl_3$ as solvent).

Table 1. The structural information of Mn(SR)2n NCs with or without guest molecules.

Series	H-G Molecules	Bonding Length (Å)			Bonding Angles (°)				Ref.
		M-M	M-S	S-α-C	M-S-M	S-M-S^a	S-M-S^e	M-S-α-C	
$Pd_8(SR)_{16}$	$Pd_8(SCH_2CH_2CH_3)_{16}$	3.23	2.32	1.84	88.05	97.77	82.27	107.06	[35]
	$Pd_8(SCH_2CO_2CH_3)_{16}$	3.23	2.32	1.82	88.20	97.69	82.71	107.20	[13]
	CH_2Cl_2@$Pd_8(SCH_2CO_2CH_3)_{16}$	3.24	2.32	1.82	88.43	97.66	82.71	107.07	[13]
	CH_2Br_2@$Pd_8(SCH_2CO_2CH_3)_{16}$	3.24	2.32	1.81	88.44	97.77	82.62	107.24	[13]
	$(CH_2Cl)_2$@$Pd_8(SCH_2CO_2CH_3)_{16}$	3.24	2.32	1.82	88.29	97.74	82.66	107.00	[13]
	CH_3I@$Pd_8(SCH_2CO_2CH_3)_{16}$	3.25	2.33	1.80	88.46	97.65	82.69	107.12	[13]
	I_2@$Pd_8(SCH_2CO_2CH_3)_{16}$	3.26	2.33	1.82	88.60	97.79	82.41	106.25	[14]
$Pt_8(SR)_{16}$	$Pt_8(SCH_2CO_2CH_3)_{16}$	3.29	2.32	1.82	90.77	98.79	81.48	107.77	[13]
	CH_2Cl_2@$Pt_8(SCH_2CO_2CH_3)_{16}$	3.29	2.33	1.82	90.37	98.04	82.11	108.22	[13]
	CH_2Br_2@$Pt_8(SCH_2CO_2CH_3)_{16}$	3.29	2.32	1.83	90.43	98.72	81.56	107.40	[13]
	$(CH_2Cl)_2$@$Pt_8(SCH_2CO_2CH_3)_{16}$	3.29	2.32	1.81	90.41	98.68	81.51	108.18	[13]
$Pt_6(SR)_{12}$	$Pt_6[S\text{-}(CH_2)_{11}\text{-}CH_3]_{12}$	3.17	2.32	1.83	86.26	98.41	81.35	108.94	[12]
	Ag@$Pt_6[S\text{-}(CH_2)_{11}\text{-}CH_3]_{12}$	3.08	2.32	1.83	83.24	97.61	82.39	109.95	[12]
Ni_{10}-(S*t*Bu)$_{10}$-(SR)$_{10}$	$Ni_{10}(S$*t*Bu)$_{10}(SC_2H_5)_{10}$	3.15	2.20	1.83	91.18	96.91	83.12	109.67	[34]
	$CH_3C_6H_5$@$Ni_{10}(S$*t*Bu)$_{10}$(etet)$_{10}$	3.21	2.22	—	93.12	96.68	82.90	—	[3]
	$CH_3C_6H_5$@$Ni_{10}(S$*t*Bu)$_{10}$(pyet)$_{10}$	3.16	2.21	1.85	91.31	97.42	83.04	109.92	[3]
	$(0.5CH_3C_6H_5)$@$Ni_{10}(S$*t*Bu)$_{10}$(atet)$_{10}$	3.17	2.21	1.85	92.06	96.96	83.07	110.02	[3]
	$Ni_{10}(S$*t*Bu)$_{10}$(mtet)$_{10}$	3.17	2.21	1.85	91.54	97.48	82.57	110.16	[11]
	C_6H_6@$Ni_{10}(S$*t*Bu)$_{10}$(mtet)$_{10}$	3.16	2.20	1.86	91.58	97.10	82.94	109.27	[11]

Noted: S*t*Bu is 2-methyl-2-propanethiol, etet is 2-ethylthioethanethiolate, pyet is 2-(2-mercaptoethyl)pyridine, atet is 2-aminoethanethiol, mtet is methylthioethanethiolate.

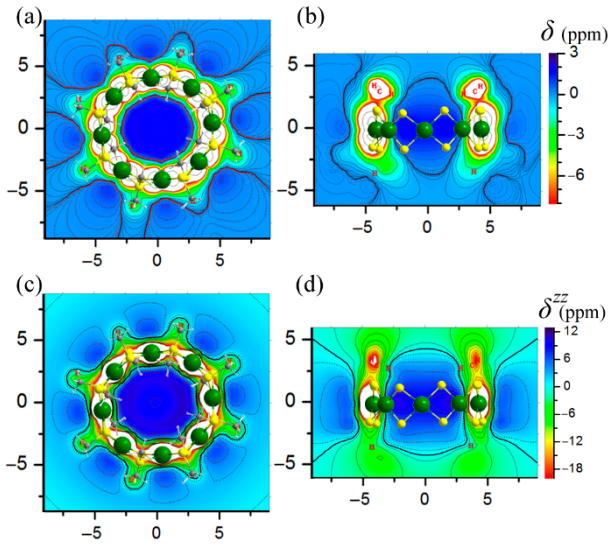

Figure 3. NICS maps $\delta_{(r)}$ (**a**,**b**) and its ZZ component $\delta^{zz}{}_{(r)}$ (**c**,**d**) denoting shielded (negative values) and deshielded (positive values) areas in ppm for $Pd_8(SCH_3)_{16}$ in perpendicular and parallel to Pd_8 ring (*xy* and *xz* contour-plane) representations.

The wider CS signal of CH_2Cl_2 in the mixture solution was caused by CH_2Cl_2 encapsulated by $Pd_8(PET)_{16}$ as well. As we know, in NMR spectrum, the total observed width of the absorption line ($\Delta\nu$) is used to define an effective relaxation time (T) by means of the relation

$$\Delta\nu \approx T^{-1}$$

where the T is mainly determined by the spin-spin relaxation time (T_2). When low concentration CH_2Cl_2 was dissolved in $CDCl_3$, the CH_2Cl_2 could effectively produce spin-lattice relaxation due to its non-restricted thermal motion but generate a slow spin-spin relaxation process because CH_2Cl_2 was mainly surrounded by $CDCl_3$; the long distance between the two H nuclei would cause a low probability of transverse relaxation. Once a CH_2Cl_2 was encapsulated into the cavity of the Pd_8S_{16} framework, its spin-lattice relaxation became more difficult due to its restricted thermal motion, but its spin-spin relaxation became faster (a shorter T_2) because of the fixed relative position between CH_2Cl_2 and $Pd_8(PET)_{16}$, and 144 hydrogen atoms in one $Pd_8(PET)_{16}$ molecule, especially 16 hydrogen atoms in the perpendicular α-CH_2 of eight 2-phenylethanethiolate ligands very close to CH_2Cl_2. The shorter T_2 would be the main factor of T for the mixture, which led to a wider absorption peak. Herein, both experimental and theoretical results show that ^{1}H NMR spectroscopy is an effective method to detect the H-G structure of CH_2Cl_2@$Pd_8(SR)_{16}$.

Finally, the size-dependent character of $M_n(SR)_{2n}$ about their H-G properties, the issue which has never been studied before, was uncovered by ^{1}H NMR spectroscopy here. Previous calculated results, which showed that several analogues of $Ni_n(SR)_{2n}$ own similar induced magnetic fields as $Pd_8(SR)_{16}$ [36], indicated that the induced magnetic fields of $M_n(SR)_{2n}$ were unrelated to their sizes and metal element species, and all $Pd_n(SR)_{2n}$ owned a similar isotropic magnetic response as $Pd_8(SR)_{16}$, which meant that the CS of the H nuclei within a guest molecule would have uniform change when the small molecule inserts into the central cavity of $Pd_n(SR)_{2n}$. To eliminate the disturbance from ligands and treated history, the series of $Pd_n(PET)_{2n}$ ($5 \leq n \leq 16$) analogues were synthesized and purified via the same process [17]. In the MALDI-TOF-MS spectrum of each $Pd_n(PET)_{2n}$ ($5 \leq n \leq 16$) (Figure 4a), the single molecular ion peak in each mass spectrum indicated that every cluster sample was pure. The ^{1}H NMR and 2D COSY spectra of CH_2Cl_2 mixed with each $Pd_n(SR)_{2n}$ are shown in Figures 4b and S3–S8. From the NMR data, one can easily find that the CS of CH_2Cl_2 in the mixture of CH_2Cl_2 and each $Pd_n(SR)_{2n}$ (n = 7, 9~16) has a similar position at 5.3 ppm and width of FWHM as pure CH_2Cl_2, except that of the mixture of

CH_2Cl_2 and $Pd_8(SR)_{16}$, indicating that only $Pd_8(SR)_{16}$ can capture a CH_2Cl_2 into its central cavity; the other sizes of $Pd_n(SR)_{2n}$ cannot form a H-G structure with CH_2Cl_2. The smaller $Pd_n(SR)_{2n}$ cannot capture CH_2Cl_2 perhaps due to their narrower central cavity, but the larger ones cannot capture CH_2Cl_2 perhaps due to the weak interaction force between the host and guest molecules that make it difficult to bind the guest molecules inserting into the larger cavity. Such results mean that a guest molecule only inserts into the matching cavity of $M_n(SR)_{2n}$, and 8 is the 'magic number' for $Pd_n(SR)_{2n}$ to capture CH_2Cl_2. The unchanged CS signal of CH_2Cl_2 mixed with smaller size $Pd_n(SR)_{2n}$, such as $Pd_7(SR)_{14}$, also indicates that the change in the CS signal of CH_2Cl_2 mixed with $Pd_8(SR)_{16}$ does not originate from CH_2Cl_2 existing in the outer deshielded area of $Pd_8(SR)_{16}$.

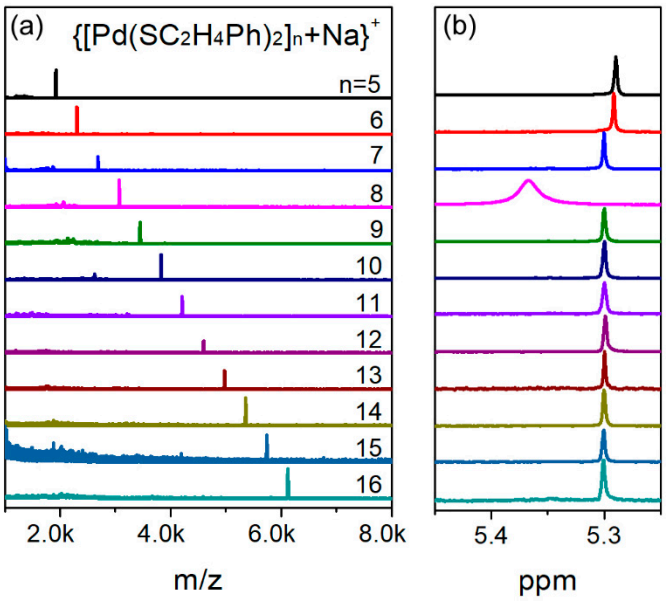

Figure 4. MALDI-TOF-MS of each $Pd_n(PET)_{2n}$ ($5 \leq n \leq 16$) (**a**) and ^1H NMR spectra in the region from 5.25 to 5.45 ppm of the mixture of CH_2Cl_2 and each $Pd_n(PET)_{2n}$ ($5 \leq n \leq 16$) (**b**).

4. Conclusions

In summary, ^1H NMR spectroscopy is shown to be a highly effective approach to confirm the H-G structure of $M_n(SR)_{2n}$. First, the result acquired by ^1H NMR spectroscopy shows that the CS of the H nuclei within CH_2Cl_2 shifts to low field (approximately 0.07 ppm) and widens when CH_2Cl_2 is mixed with $Pd_8(PET)_{16}$ in a $CDCl_3$ solution. Then, the deshielded effect in the inner void of the double-crown $Pd_8(SR)_{16}$ was clarified via the NICS procedure, which indicated that the CS of the nucleus within a small molecule will theoretically move towards low field when the guest molecule inserts into the cluster. The faster transverse relaxation process between the hydrogen nuclei of the guest CH_2Cl_2 and host $Pd_8(PET)_{16}$ leads to a wider CS signal of the hydrogen nuclei within CH_2Cl_2. Both the experimental and theoretical results indicated that ^1H NMR spectroscopy is a powerful tool to probe the H-G property of $M_n(SR)_{2n}$. Finally, we find that $Pd_8(SR)_{16}$ is the only NC in the series of $Pd_n(SR)_{2n}$ analogues that can capture a CH_2Cl_2 in its central cavity, showing that the H-G properties of $M_n(SR)_{2n}$ are highly dependent on their cavity size, and a guest molecule just inserts into the matching cavity of $M_n(SR)_{2n}$. This research provides an alternative strategy to study the H-G properties of thiolate-protected tiara-like structural $M_n(SR)_{2n}$ nanoclusters.

Supplementary Materials: The following supporting information can be downloaded at: https://www.mdpi.com/article/10.3390/pr10122683/s1, Figure S1: the MALDI-TOF-MS spectrum of $Pd_8(PET)_{16}$; Figure S2: The ^1H NMR spectra of pure $Pd_8(PET)_{16}$, the mixture of CH_2Cl_2+$Pd_8(PET)_{16}$ and pure CH_2Cl_2; Figure S3: ^1H NMR and COSY spectra of $Pd_5(PET)_{10}$; Figure S4: ^1H NMR and COSY spectra of $Pd_6(PET)_{12}$; Figure S5: ^1H NMR spectrum of $Pd_7(PET)_{14}$ and the comparison of the

^{1}H NMR spectra of $Pd_7(PET)_{14}$ and $Pd_6(PET)_{12}$ in the aliphatic regio; Figure S6: ^{1}H NMR spectrum of $Pd_9(PET)_{18}$ and the comparison of the ^{1}H NMR spectra of $Pd_9(PET)_{18}$ and $Pd_8(PET)_{16}$ in the aliphatic region; Figure S7: ^{1}H NMR and COSY spectra of $Pd_{10}(PET)_{20}$; Figure S8: ^{1}H NMR spectra of $Pd_n(PET)_{2n}$ ($11 \leq n \leq 16$) in the range of 0~8 and 2~4.

Author Contributions: Methodology, C.Z.; software, S.G.; writing—original draft preparation, J.C.; writing—review and editing, Z.W. All authors have read and agreed to the published version of the manuscript.

Funding: This work was financially supported by the China Postdoctoral Science Foundation (2016M602093) and Natural Science Foundation of Shandong (ZR2020MB063) and the Taishan Scholar Program of Shandong Province (No. ts201511027).

Conflicts of Interest: The authors declare no conflict of interest.

References

1. Imaoka, T.; Akanuma, Y.; Haruta, N.; Tsuchiya, S.; Ishihara, K.; Okayasu, T.; Chun, W.-J.; Takahashi, M.; Yamamoto, K. Platinum clusters with precise numbers of atoms for preparative-scale catalysis. *Nat. Commun.* **2017**, *8*, 688. [CrossRef] [PubMed]
2. Ananikov, V.P.; Orlov, N.V.; Zalesskiy, S.S.; Beletskaya, I.P.; Khrustalev, V.N.; Morokuma, K.; Musaev, D.G. Catalytic adaptive recognition of thiol (SH) and selenol (SeH) groups toward synthesis of functionalized vinyl monomers. *J. Am. Chem. Soc.* **2012**, *134*, 6637–6649. [CrossRef] [PubMed]
3. Zhang, C.; Matsumoto, T.; Samoc, M.; Petrie, S.; Meng, S.; Corkery, T.C.; Stranger, R.; Zhang, J.; Humphrey, M.G.; Tatsumi, K. Dodecanuclear-ellipse and decanuclear-wheel nickel(II) thiolato clusters with efficient femtosecond nonlinear absorption. *Angew. Chem. Int. Ed.* **2010**, *49*, 4209–4212. [CrossRef] [PubMed]
4. Tafen, D.N.; Kauffman, D.R.; Alfonso, D.R. Electrocatalytic oxygen evolution with pure and substituted $M_6(SR)_{12}$ (M = Pd, Fe, Rh) complexes. *Comput. Mater. Sci.* **2018**, *150*, 283–290. [CrossRef]
5. Chen, J.; Pan, Y.; Wang, Z.; Zhao, P. The fluorescence properties of tiara like structural thiolated palladium clusters. *Dalton Trans.* **2017**, *46*, 12964–12970. [CrossRef]
6. Zhu, M.; Zhou, S.; Yao, C.; Liao, L.; Wu, Z. Reduction-resistant and reduction-catalytic double-crown nickel nanoclusters. *Nanoscale* **2014**, *6*, 14195–14199. [CrossRef]
7. Zhuang, Z.; Yang, Q.; Chen, W. One-step rapid and facile synthesis of subnanometer-sized $Pd_6(C_{12}H_{25}S)_{11}$ clusters with ultra-high catalytic activity for 4-nitrophenol reduction. *ACS Sustain. Chem. Eng.* **2019**, *7*, 2916–2923. [CrossRef]
8. Joya, K.S.; Sinatra, L.; AbdulHalim, L.G.; Joshi, C.P.; Hedhili, M.N.; Bakr, O.M.; Hussain, I. Atomically monodisperse nickel nanoclusters as highly active electrocatalysts for water oxidation. *Nanoscale* **2016**, *8*, 9695–9703. [CrossRef]
9. Woodward, P.; Dahl, L.F.; Abel, E.W.; Crosse, B.C. A new type of cyclic transition metal complex, $[Ni(SC_2H_5)_2]_6$. *J. Am. Chem. Soc.* **1965**, *87*, 5251–5253. [CrossRef]
10. Ivanov, S.A.; Kozee, M.A.; Merrill, W.A.; Agarwal, S.; Dahl, L.F. *Cyclo*-$[Ni(\mu_2\text{-}SPh)_2]_9$ and *cyclo*-$[Ni(\mu_2\text{-}SPh)_2]_{11}$: New oligomeric types of toroidal nickel(II) thiolates containing geometrically unprecedented 9- and 11-membered ring systems. *J. Chem. Soc. Dalton Trans.* **2002**, *22*, 4105–4115. [CrossRef]
11. Zhang, C.; Takada, S.; Kölzer, M.; Matsumoto, T.; Tatsumi, K. Nickel(II) thiolate complexes with a flexible cyclo-$\{Ni_{10}S_{20}\}$ framework. *Angew. Chem. Int. Ed.* **2006**, *45*, 3768–3772. [CrossRef] [PubMed]
12. Shichibu, Y.; Yoshida, K.; Konishi, K. Hexanuclear platinum(II) thiolate macrocyclic host: Charge-transfer-driven inclusion of a Ag^I ion guest. *Inorg. Chem.* **2016**, *55*, 9147–9149. [CrossRef] [PubMed]
13. Yamashina, Y.; Kataoka, Y.; Ura, Y. Tiara-like octanuclear palladium(II) and platinum(II) thiolates and their inclusion complexes with dihalo- or iodoalkanes. *Inorg. Chem.* **2014**, *53*, 3558–3567. [CrossRef] [PubMed]
14. Yamashina, Y.; Kataoka, Y.; Ura, Y. Inclusion of an iodine molecule in a tiara-like octanuclear palladium thiolate complex. *Eur. J. Inorg. Chem.* **2014**, *2014*, 4073–4078. [CrossRef]
15. Pan, Y.; Chen, J.; Gong, S.; Wang, Z. Co-synthesis of atomically precise nickel nanoclusters and the pseudo-optical gap of $Ni_4(SR)_8$. *Dalton Trans.* **2018**, *47*, 11097–11103. [CrossRef]
16. Dance, I.G.; Scudder, M.L.; Secomb, R. *c*-$Ni_8(SCH_2COOEt)_{16}$, a receptive octagonal toroid. *Inorg. Chem.* **1985**, *24*, 1201–1208. [CrossRef]
17. Chen, J.; Liu, L.; Weng, L.; Lin, Y.; Liao, L.; Wang, C.; Yang, J.; Wu, Z. Synthesis and properties evolution of a family of tiara-like phenylethanethiolated palladium nanoclusters. *Sci. Rep.* **2015**, *5*, 16628. [CrossRef]
18. Mezei, G.; Zaleski, C.M.; Pecoraro, V.L. Structural and functional evolution of metallacrowns. *Chem. Rev.* **2007**, *107*, 4933–5003. [CrossRef]
19. Sobiech, T.A.; Zhong, Y.; Miller, D.P.; McGrath, J.K.; Scalzo, C.T.; Redington, M.C.; Zurek, E.; Gong, B. Ultra-tight host-guest binding with exceptionally strong positive cooperativity. *Angew. Chem. Int. Ed.* **2022**, *61*, e202213467. [CrossRef]
20. Hu, S.-J.; Guo, X.-Q.; Zhou, L.-P.; Yan, D.-N.; Cheng, P.-M.; Cai, L.-X.; Li, X.-Z.; Sun, Q.-F. Guest-driven self-assembly and chiral induction of photofunctional lanthanide tetrahedral cages. *J. Am. Chem. Soc.* **2022**, *144*, 4244–4253. [CrossRef]

21. Schäfer, F.; Mix, A.; Cati, N.; Lamm, J.-H.; Neumann, B.; Stammler, H.-G.; Mitzel, N.W. Host-guest chemistry of a bidentate silyl-triflate bis-Lewis acid—Complex complexation behaviour unravelled by diffusion NMR spectroscopy. *Dalton Trans.* **2022**, *51*, 7164–7173. [CrossRef] [PubMed]
22. Boles, J.E.; Bennett, C.; Baker, J.; Hilton, K.L.F.; Kotak, H.A.; Clark, E.R.; Long, Y.; White, L.J.; Lai, H.Y.; Hind, C.K.; et al. Establishing the selective phospholipid membrane coordination, permeation and lysis properties for a series of 'druggable' supramolecular self-associating antimicrobial amphiphiles. *Chem. Sci.* **2022**, *13*, 9761–9773. [CrossRef]
23. Mi, Y.; Ma, J.; Liang, W.; Xiao, C.; Wu, W.; Zhou, D.; Yao, J.; Sun, W.; Sun, J.; Gao, G.; et al. Guest-binding-induced interhetero hosts charge transfer crystallization: Selective coloration of commonly used organic solvents. *J. Am. Chem. Soc.* **2021**, *143*, 1553–1561. [CrossRef] [PubMed]
24. Wong, Y.-S.; Ng, M.; Yeung, M.C.-L.; Yam, V.W.-W. Platinum(II)-based host–guest coordination-driven supramolecular Co-assembly assisted by Pt···Pt and π–π stacking interactions: A dual-selective luminescence sensor for cations and anions. *J. Am. Chem. Soc.* **2021**, *143*, 973–982. [CrossRef] [PubMed]
25. Frisch, M.J.; Trucks, G.W.; Schlegel, H.B.; Scuseria, G.E.; Robb, M.A.; Cheeseman, J.R.; Scalmani, G.; Barone, V.; Petersson, G.A.; Nakatsuji, H.; et al. *Gaussian 16, Revision B.01*; Gaussian, Inc.: Wallingford, UK, 2016.
26. Wilson, P.J.; Bradley, T.J.; Tozer, D.J. Hybrid exchange-correlation functional determined from thermochemical data and *ab initio* potentials. *J. Chem. Phys.* **2001**, *115*, 9233–9242. [CrossRef]
27. Flaig, D.; Maurer, M.; Hanni, M.; Braunger, K.; Kick, L.; Thubauville, M.; Ochsenfeld, C. Benchmarking hydrogen and carbon NMR chemical shifts at HF, DFT, and MP2 levels. *J. Chem. Theory Comput.* **2014**, *10*, 572–578. [CrossRef] [PubMed]
28. Jensen, F. Segmented contracted basis sets optimized for nuclear magnetic shielding. *J. Chem. Theory Comput.* **2015**, *11*, 132–138. [CrossRef]
29. Andrae, D.; Haussermann, U.; Dolg, M.; Stoll, H.; Preuss, H. Energy-adjusted *ab initio* pseudopotentials for the second and third row transition elements. *Theor. Chim. Acta* **1990**, *77*, 123–141. [CrossRef]
30. Chen, Z.; Wannere, C.S.; Corminboeuf, C.; Puchta, R.; Schleyer, P.V.R. Nucleus-independent chemical shifts (NICS) as an aromaticity criterion. *Chem. Rev.* **2005**, *105*, 3842. [CrossRef]
31. Lu, T.; Chen, F. Multiwfn: A multifunctional wavefunction analyzer. *J. Comput. Chem.* **2012**, *33*, 580–592. [CrossRef]
32. Kagalwala, H.N.; Gottlieb, E.; Li, G.; Li, T.; Jin, R.; Bern-hard, S. Photocatalytic hydrogen generation system using a nickel-thiolate hexameric cluster. *Inorg. Chem.* **2013**, *52*, 9094–9101. [CrossRef] [PubMed]
33. Gottlieb, H.E.; Kotlyar, V.; Nudelman, A. NMR chemical shifts of common laboratory solvents as trace impurities. *J. Org. Chem.* **1997**, *62*, 7512–7515. [CrossRef] [PubMed]
34. Tan, C.; Jin, M.; Ma, X.; Zhu, Q.; Huang, Y.; Wang, Y.; Hu, S.; Sheng, T.; Wu, X. In situ synthesis of nickel tiara-like clusters with two different thiolate bridges. *Dalton Trans.* **2012**, *41*, 8472–8476. [CrossRef]
35. Higgins, J.D.; William Suggs, J. Preparation, structure and spectroscopic studies of the palladium mercaptides Pd_8(S-nPr)$_{16}$ and Pd_6(S-nPr)$_{12}$. *Inorg. Chim. Acta* **1988**, *145*, 247–252. [CrossRef]
36. Muñoz-Castro, A. Bonding and magnetic response properties of several toroid structures. Insights of the role of Ni2S2 as a building block from relativistic density functional theory calculations. *J. Phys. Chem. A* **2011**, *115*, 10789–10794. [CrossRef] [PubMed]